



Originally published as:

Domingues, A., Custodio, S., Cesca, S. (2013): Waveform inversion of small-to-moderate earthquakes located offshore southwest Iberia. - *Geophysical Journal International*, 192, 1, pp. 248—259.

DOI: <http://doi.org/10.1093/gji/ggs010>

Waveform inversion of small-to-moderate earthquakes located offshore southwest Iberia

A. Domingues,^{1,2} S. Custódio² and S. Cesca³

¹ICIST, Instituto Superior Técnico, 1049-001 Lisboa, Portugal. E-mail: susanacustodio@dct.uc.pt

²Centro de Geofísica, Universidade de Coimbra, 3030-134 Coimbra, Portugal

³Institut für Geophysik, Universität Hamburg, D-20146 Hamburg, Germany

Accepted 2012 October 5. Received 2012 September 28; in original form 2012 April 12

SUMMARY

In this paper we apply the Kinematic Waveform Inversion (KIWI) tools to the study of small-to-moderate earthquakes in southwest (SW) Iberia. The earthquakes have magnitudes in the range M_L 3.5–4.9, with the exception of one earthquake with magnitude M_L 6.0. Most events are located offshore, are recorded with a large azimuthal gap and generate waves that travel through a strongly heterogeneous crustal structure. We obtain new estimates of centroid, depth, seismic moment, strike, dip and rake for 12 of the 29 studied events. The earthquakes whose waveforms we cannot successfully model are (1) located too far from the stations, (2) have small magnitude, hence low signal-to-noise ratio or (3) are located within the Cadiz basin, which is a major sedimentary basin that affects wave propagation notably. Our results indicate that onshore earthquakes occur at shallow depths (<15 km), whereas offshore earthquakes occur deeper, down to 46 km. Focal mechanisms indicate transpressive faulting.

Key words: Inverse theory; Earthquake source observations; Seismicity and tectonics.

1 INTRODUCTION

A proper characterization of earthquake sources is fundamental to understanding tectonics and earthquake dynamics. Magnitude and source location are the main requirements for a first-order characterization of an earthquake. Information on the faulting style and finite-fault parameters, such as rupture area and spatiotemporal evolution of slip, complete the description of the event. The most general and widely used representation of a seismic point-source is the moment tensor (MT) \mathbf{M} (Gilbert 1971; Aki & Richards 1980). Style of faulting (or focal mechanism) and scalar seismic moment are some of the source parameters that can be extracted from the MT. The use of regional data allows the study of MTs for earthquakes with magnitudes down to M_w 3.5 (e.g. Nakanishi *et al.* 1992; Giardini *et al.* 1993; Ritsema & Lay 1993). In Europe, several institutions currently compute MTs from regional data. Some of the MT catalogues are based on fully automated methods, while others require manual input. Most of these catalogues are available through the website of the Euro-Mediterranean Seismological Centre (EMSC; <http://www.emsc-csem.org/Earthquake/tensors.php>).

Cesca *et al.* (2006) improved the stability of local and regional earthquake source studies by developing a method that combines frequency- and time-domain analysis. The authors showed that their approach performed better than simple time-domain inversion both in the presence of crustal structure inaccuracies and large azimuthal gaps. They also showed that the proposed method was stable up to frequencies higher than those normally used for time-domain inversion. The approach of Cesca *et al.* (2006) was partially adopted in

the Kinematic Waveform Inversion (KIWI) Tools (Heimann 2011), which provide accurate estimates of depth, centroid location, seismic moment, strike, dip and rake based on waveform data. For large enough earthquakes, simplified kinematic finite-fault models can also be generated. The KIWI tools have a modular structure that allows easy implementation and use of different inversion algorithms, misfit measures, frequency passbands, portions of the waveform, etc. Another advantage over common time-domain inversion is that no waveform alignment is required in advance, because the inversion for focal mechanisms is based on amplitude spectra. KIWI is designed to be easily implemented in real time, and a plug-in for Seiscomp 3.0 (<http://www.seiscomp3.org/>) already exists. Cesca *et al.* (2010) tested the KIWI tools with regional data from Greece (M_w 5.1–6.8) and local data from Germany (M_w 3.4–4.8). Custódio *et al.* (2012) used the KIWI tools to study the 2007 M_w 5.9 Horseshoe Abyssal Plain, which occurred offshore southwest (SW) Iberia. In this paper, we apply the KIWI tools to a set of small-to-moderate earthquakes in SW Iberia. The real-time implementation of KIWI to monitor the Portuguese seismicity is ongoing.

The seismicity of SW Iberia is governed by the nearby collision of the Eurasia and African plates. The WNW–ESE convergence between Iberia and Nubia occurs at a slow rate of 4–5 mm yr⁻¹ (Argus *et al.* 1989; DeMets *et al.* 1994; Calais *et al.* 2003; Fernandes *et al.* 2003; McClusky *et al.* 2003; Nocquet & Calais 2004; Serpelloni *et al.* 2007; Fernandes *et al.* 2007). This convergence is accommodated along a broad belt of distributed deformation and structural complexity, which encompasses the epicentral area of the largest historical European earthquake: the M 8.5–8.7 1755

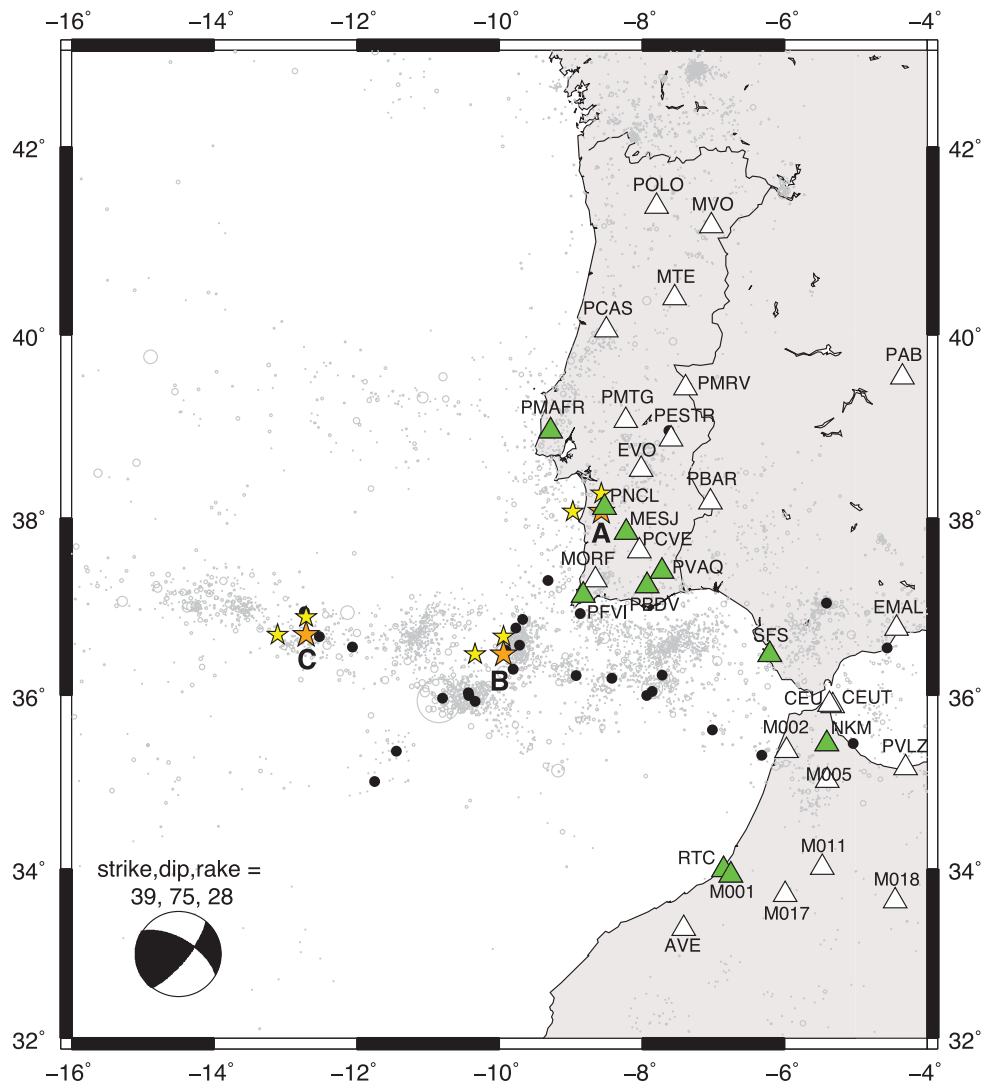


Figure 1. Map showing studied earthquakes (black dots) and used stations (triangles). Setup of the synthetic tests: stations (green triangles), test epicentres A, B and C (orange stars) and incorrect starting epicentres (yellow stars). The background seismicity in the instrumental (post-1961) catalogue is displayed by grey circles (Carrilho *et al.* 2004; Preliminary Seismic Information 2010; Pena *et al.* in press). The test focal mechanism is shown on the lower left corner.

great Lisbon earthquake (Johnston 1996; Martinez Solares & Lopez Arroyo 2004). Present catalogues show diffuse seismicity offshore SW Iberia, which does not delineate individual faults (Fig. 1). Whether the seismicity is in fact diffuse or just poorly located remains an open question. The two largest earthquakes in the instrumental record are an M_S 7.9 earthquake in 1969 (Fukao 1973) and an M_w 5.9 earthquake in 2007 (Stich *et al.* 2007; Custódio *et al.* 2012). For a thorough discussion of the seismotectonics of SW Iberia we refer the readers to Borges *et al.* (2001), Buforn *et al.* (2004), Serpelloni *et al.* (2007), Zitellini *et al.* (2009), Stich *et al.* (2010), and references therein.

Earthquakes in SW Iberia are particularly challenging to study because most active sources are located offshore, at large distances (>100 km) from the coast (Fig. 1). Moderate-to-small earthquakes are commonly recorded with a large azimuthal gap that leads to errors in traveltime-based epicentral locations and focal depths. Geissler *et al.* (2010) used data from an ocean bottom seismometer (OBS) network temporarily deployed in the Gulf of Cadiz to characterize the local seismicity. The authors showed that land-estimated epicentres (computed with data recorded at the land stations) were

mislocated by up to 50 km with respect to OBS-estimated epicentres. The land-estimated focal depths were also considerably shallower than those estimated from OBS data, with differences up to 40 km. The OBS-estimated depths are on the order of 40–60 km, with a pronounced peak at 50 km, suggesting an unusually thick seismogenic layer. The low temperature of the old lithosphere has been proposed as the cause for the thick seismogenic layer (McKenzie *et al.* 2005; Stich *et al.* 2007). A proper knowledge of the depth of the seismogenic layer, as well as of seismogenic structures, is important for understanding, modelling and/or simulating large ruptures such as the 1755 Lisbon earthquake. Reliable depth and epicentre estimates of regional earthquakes are key to understanding the seismogenic and tsunamigenic hazard of SW Iberia.

In this paper we use the KIWI tools to study the source mechanism of 29 regional earthquakes with M_L 3.5–6.0 that occurred between 2007 and 2010. Most of the events are located offshore SW Iberia. The data were recorded by broadband (BB) stations in Portugal, Spain and Morocco. The waveform inversion of these events is performed in adverse conditions and provides a good check on the performance of the KIWI tools. Challenges to waveform

inversion include: (1) Small magnitude of the earthquakes. Portugal is exposed to moderate and large magnitude earthquakes, however the tectonic rate is slow, leading to a low rate of seismic activity (long recurrence intervals; Vilanova & Fonseca 2007; Fernandes *et al.* 2007, and references therein); (2) poor azimuthal coverage; (3) laterally heterogeneous Earth structure. Most earthquakes occur in the Cadiz Basin, which is a major sedimentary basin (Thiebot & Gutscher 2006) that strongly affects wave propagation. The transition from oceanic to continental crust further challenges the use of simple 1-D earth models. We start by performing synthetic tests to assess the performance of the KIWI tools in the source–station configuration of SW Iberia. Next, we invert real data. We assign a quality factor to each event, from A (best quality) to D (poorest quality). We report 12 solutions with reliable qualities A and B. From these 12 events, only 4 have previously published focal mechanisms.

2 DATA

Table 1 lists the earthquakes studied and Fig. 1 shows the epicentres and seismic stations. The 29 studied events are those listed in the Portuguese earthquake catalogue with $M_L > 3.5$ that occurred after 2007, when the Portuguese BB network was upgraded. Data were collected from BB stations in Portugal and neighbour countries (Table 2 and Fig. 1). We considered all available data recorded both at permanent stations and at the temporary stations of project Topolberia (Díaz *et al.* 2010). Only two of the 29 earthquakes are located in mainland Portugal (M_L 3.8 and 4.1). Magnitudes vary in the range M_L 3.5–4.9, with one exception: the M_L 6.0 earthquake of 2009 December 17. The waveforms were imported in SAC format and pre-processed according to the following procedure: (1)

removal of mean and linear trend; (2) deconvolution of instrumental response; (3) bandpass filtering and (4) decimation to 0.2 s. Earthquakes with $M_L \leq 4.2$ were filtered in the passband 0.05–0.1 Hz, and earthquakes with $M_L > 4.2$ in the passband 0.025–0.1 Hz. As an exception, event 070701 was filtered in the passband 0.025–0.08 Hz. The high-frequency content of this event was not usable in the inversion, probably due to its distance from the stations.

3 METHOD

A priori estimates (or initial guesses) of earthquake epicentre, depth and magnitude are required as inputs to KIWI. We use as inputs the parameters provided by the catalogue of Instituto de Meteorologia (IM; Preliminary Seismic Information 2010), which is the catalogue that relies on the largest amount of near-source data. These inputs are also the ones available in our regional real-time implementation of KIWI. The first step performed by KIWI is an inversion of amplitude spectra that retrieves strike, dip, rake, scalar moment and improved depth estimate. We minimize the misfit between observed and synthetic amplitude spectra, using the L2 norm in a Levenberg–Marquardt inversion scheme. Given that only amplitude spectra are analysed, the polarity information is discarded, and the compressive and dilatational quadrants cannot be distinguished. After concluding this first step we obtain four possible configurations for strike, dip and rake.

Next, the centroid coordinates (latitude and longitude) and earthquake onset time are retrieved by inverting data in the time domain. In this second stage, the parameters retrieved during the first step are held fixed, and the bandpass filtered time-domain seismograms are shifted and compared with synthetics to obtain the proper centroid location and origin time. Again, we use full waveforms and use the

Table 1. List of 29 earthquakes studied in this paper (Preliminary Seismic Information 2010).

ID	Date	Time	Latitude (°N)	Longitude (°E)	Depth (km)	M_L
070217	17-02-2007	05:44:00	36.000	−10.431	33	3.7
070306	06-03-2007	07:50:52	35.363	−11.446	25	3.7
070410	10-04-2007	19:46:28	36.931	−8.869	28	3.5
070701	01-07-2007	19:03:14	36.554	−12.066	10	4.9
071106	06-11-2007	23:09:53	36.231	−8.925	4	3.7
080111	11-01-2008	00:21:45	36.480	−9.944	17	4.7
080414	14-04-2008	03:33:08	37.304	−9.317	25	3.7
080510	10-05-2008	16:33:07	35.970	−10.801	20	4.1
080717	17-07-2008	19:22:06	36.301	−9.806	6	3.8
080909	09-09-2008	13:36:41	35.610	−7.017	20	3.9
081002	02-10-2008	04:02:54	37.050	−5.416	14	4.7
090217	17-02-2009	16:00:05	38.070	−8.570	6	3.8
090522	22-05-2009	23:58:08	36.863	−9.676	21	3.6
090705	05-07-2009	15:50:58	36.035	−10.436	31	4.4
090818	18-08-2009	06:56:04	36.049	−7.860	31	4.2
090905	05-09-2009	00:47:32	36.668	−12.527	10	4.2
090908	08-09-2009	00:04:05	36.000	−7.938	31	4.0
090918	18-09-2009	01:27:09	36.574	−9.719	31	3.7
091030	30-10-2009	07:01:06	36.544	−4.561	78	3.9
091217	17-12-2009	01:37:52	36.516	−9.909	31	6.0
100305	05-03-2010	17:10:50	36.200	−8.424	11	3.9
100307	07-03-2010	16:35:15	35.453	−5.037	20	3.7
100327	27-03-2010	13:37:53	38.964	−7.624	13	4.1
100331	31-03-2010	03:12:03	36.769	−9.769	20	4.2
100422	22-04-2010	01:24:02	35.320	−6.321	31	4.2
100723	23-07-2010	12:45:17	35.934	−10.340	31	3.9
100725	25-07-2010	20:24:41	36.235	−7.717	10	3.9
101108	08-11-2010	06:55:48	35.013	−11.753	31	3.7
101129	29-11-2010	23:57:28	36.951	−12.736	10	4.0

Table 2. Broad-band stations used in this study.

Station	Network	Longitude (°W)	Latitude (°N)
AVE	WM	7.413	33.298
CEU	WM	5.373	35.899
CEUT	IG	5.326	35.883
EMAL	WM	4.428	36.762
EVO	WM	8.017	38.529
M001	IB	6.756	33.929
M002	IB	5.971	35.37
M005	IB	5.403	35.028
M007	IB	3.801	34.756
M011	IB	5.472	34.017
M014	IB	3.837	33.940
M017	IB	5.991	33.699
M018	IB	4.449	33.623
MELI	GE	2.935	35.294
MESJ	LX	8.22	37.84
MORF	LX	8.651	37.306
MTE	GE	7.537	40.403
MVO	PM	7.029	41.165
NKM	IB	5.41	35.448
PAB	IU	4.348	39.546
PBAR	PM	7.039	38.175
PBDV	PM	7.931	37.243
PCAS	PM	8.498	40.053
PCVE	PM	8.039	37.633
PESTR	PM	7.59	38.867
PFVI	PM	8.827	37.133
PMAFR	PM	9.283	38.955
PMRV	PM	7.392	39.428
PMTG	PM	8.225	39.069
PNCL	PM	8.529	38.112
POLO	PM	7.794	41.374
PVAQ	PM	7.717	37.404
PVLZ	WM	4.301	35.173
RTC	MN	6.857	33.988
SELV	IG	3.728	37.238
SFS	GE	6.206	36.466
TA07	IB	2.383	37.021

L2 norm, now in a grid walk inversion. Waveform polarities allow the retrieval of the information on compressional and dilatational quadrants, reducing the number of possible combinations of strike, dip and rake to two (true and auxiliary fault planes).

Finally, a third step in the algorithm serves to compute finite source parameters such as true fault plane, source dimension, nucleation coordinates (and ensuing directivity) and rupture velocity. At this stage, full waveforms including higher frequencies must be used. This last step will not be applied in this paper due to the low magnitude of the studied earthquakes.

Forward modelling of synthetic displacements corresponding to trial sources is inherent to any iterative inversion scheme. The inversion performed by KIWI is expedited by using a database of Green's functions (GFs) computed in advance (Cesca *et al.* 2006; Heimann 2011). The component n of ground displacement u at a particular site can be conveniently written as (Aki & Richards 1980):

$$u_n(t) = \int m_{pq} * G_{np,q} dA. \quad (1)$$

In the equation above, m_{pq} are the MT components, which depend on slip and fault orientation, and $G_{np,q}$ are spatial derivatives of the GFs, which depend on the crustal structure and on the location of the stations with respect to the source. The integration is performed over the area A where slip occurs and '*' represents time

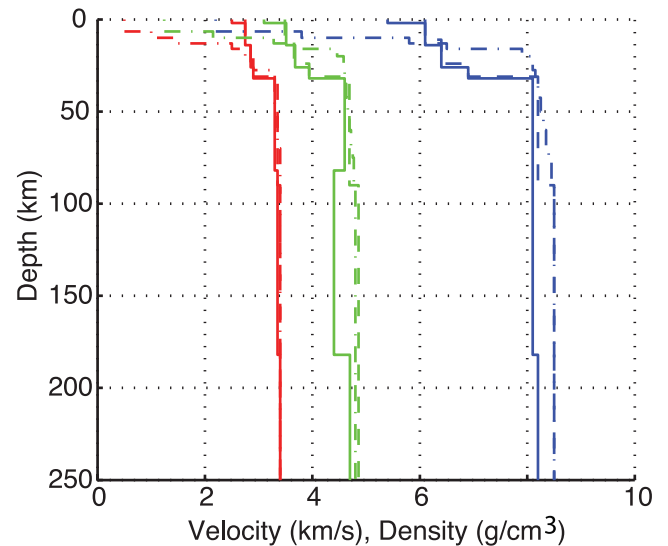


Figure 2. Crustal models used in the synthetic test: model S (full lines), model I (dashed lines) and model G (dash-dot lines). The figure displays V_P (blue), V_S (green) and ρ (red).

convolution. The GFs database contains all the GFs for a grid of epicentral distances and source depths. We compute 1-D GFs using a reflectivity method implemented in QSEIS (Wang 1999), which is based on the Thomson–Haskell propagator algorithm (Thomson 1950; Haskell 1953). We adopt a general layered crustal model proposed for ray paths in the Hercynian basement, continental platform and a mix of both (Stich *et al.* 2003, see Fig. 2, model S). The GFs database has a uniform grid spacing of 1 km with a range of source depths from 1 to 80 km and epicentral distances range from 1 to 600 km. GFs are linearly interpolated between grid nodes. 3-D GFs are currently being implemented in KIWI.

In this study we use the L2 norm to measure the misfit M between recorded (data) and synthetic ground motion:

$$M = \frac{\sum_i (u_i^{\text{syn}} - u_i^{\text{obs}})^2}{\sum_i (u_i^{\text{obs}})^2}. \quad (2)$$

In the equation above, u_i^{obs} and u_i^{syn} are observed and synthetic displacements, respectively, for station-component i .

To separate good solutions from poor solutions we attributed a quality factor to each event, ranging from A (best quality) to D (poorest quality). The quality factor is based on the misfit from inversion step 1, misfit from inversion step 2 and number of stations used in the inversion (Table 3). According to this criterion, inversions that use more stations and have lower misfits in both steps are given a better quality factor. We further apply a second criterium based on bootstrap analysis. When the probability of any of the

Table 3. Criterium used to distinguish the quality of the solutions. Misfit 1 and Misfit 2 correspond to the misfit measured between the synthetics and the observed data in step 1 and step 2 of the method, respectively.

	Misfit 1	Misfit 2	No. of stations
Quality A	<0.450	<0.900	≥ 7
Quality B	<0.500	<1.050	≥ 6
Quality C	<0.600	<1.200	≥ 5
Quality D	<0.700	<1.500	≥ 4

source parameters, as inferred from bootstrap, is lower than 30 per cent, the solution is considered unreliable.

4 SYNTHETIC TESTS

Given perfect (noiseless) data, how appropriate is the inversion algorithm to study the seismicity of SW Iberia? In this section we present the results of synthetic tests. We choose a source model, forward compute ground motion at given station components (which we will refer to as ‘perfect data’) and invert the ‘perfect data’. We then compare the output source model with the initial input. We repeat this procedure in different configurations to assess the effects of erroneous crustal structure, station coverage/azimuthal gap, and incorrect starting values of epicentre and depth (Fig. 1). Noise is not added to the synthetic waveforms before running the inversions because our goal is not to focus on the effect of noise in data but rather on the effect of erroneous starting parameters and crustal structure. In all synthetic tests, the following parameters are held fixed:

- (i) Source time function. The source time function is a triangle with a width of 1 s, which is the shortest duration allowed by the GFs sampling.
- (ii) Seismic moment. The seismic moment M_0 is set to 1.5×10^{15} N m, which corresponds to a moment magnitude $M_w = 4.0$.
- (iii) Focal mechanism. We take the focal mechanism of event 080111 as our reference source: (strike, dip, rake) = (39°, 75°, 28°) and (301°, 63°, 164°). The focal mechanism of this event is well known (Geissler *et al.* 2010; Stich *et al.* 2010, and Instituto Geográfico Nacional Catalogue).
- (iv) Frequency passband. Waveforms are filtered in the passband 0.025–0.1 Hz.
- (v) Stations. We use three-component ‘perfect data’ computed at 10 stations in Portugal, Spain and Morocco: PFVI, PBDV, PNCL, PMAFR, PVAQ, MESJ, SFS, M002, RTC, NKM (Fig. 1).
- (vi) Crustal model. ‘Perfect data’ are always generated using the crustal model proposed by Stich *et al.* (2003) (model S in Fig. 2).

The inversions of ‘perfect data’ are carried out in the following configurations:

- (i) Crustal structure. We invert the ‘perfect data’ using three different crustal models (Fig. 2). All models consist of horizontal layers characterized by thickness, velocity of P and S waves (V_P and V_S), density (ρ) and attenuation of P and S waves ($1/Q_P$ and $1/Q_S$). The three different models are:

- (1) Model S, proposed by Stich *et al.* (2003).
- (2) Model I, corresponding to model IMG used by IM for routine epicentral location of offshore events on the continental shelf.
- (3) Model G, used by Geissler *et al.* (2010), which includes a shallow layer of sediments that is adequate for the Cadiz Basin.

- (ii) Epicentral location and station coverage/azimuthal gap. We study ‘perfect data’ generated by three different events (orange stars in Fig. 1) and recorded at stations with a maximum epicentral distance of 500 km. Thus the number of stations used in each inversion and the azimuthal gap depend on the position of the test epicentre. The three studied epicentres are:

- (1) Epicentre A (onshore): 38.07°N, 8.57°W, after event 090217. ‘Perfect data’ are generated at nine stations and the azimuthal gap is 162°.

- (2) Epicentre B (offshore, close to land): 36.47°N, 9.94°W, after event 080111. ‘Perfect data’ are generated at 10 stations and the azimuthal gap is 238°.

- (3) Epicentre C (offshore, far from land): 36.69°N, 12.71°W, after event 090905. ‘Perfect data’ are generated at five stations and the azimuthal gap is 329°.

- (iii) Incorrect starting location. We considered the following cases:

- (1) Depth. We considered true depths of 10, 40 and 60 km, and an incorrect starting depth of 30 km.
- (2) Epicentre. We considered starting epicentres deviated by 0.2°N (~ 20 km) and 0.4°W (~ 35 km) of the reference epicentres (yellow stars in Fig. 1).

Fig. 3 summarizes the results of the synthetic tests. Figs 3(a)–(c) show the results obtained using different crustal models and correct starting hypocentres. When we invert ‘perfect data’ using the crustal models S and I, we obtain the correct focal mechanisms. In fact, models S and I are quite similar. Because model S was used in the first place to generate the ‘perfect data’, results using models S and I are good. Model G has shallow low-velocity layers that generate very energetic surface waves, which are difficult to fit to waveforms generated with model S. This result indicates that an incorrect crustal structure will impact considerably the solutions. Note we are not assessing which model is more appropriate, solely assessing the impact of an erroneous crustal model in the inversion.

Figs 3(d)–(h) show the results of synthetic tests using incorrect starting locations. In most situations we obtain well-resolved focal mechanisms. Notably, some disagreement is obtained for the onshore event A. At step 1, KIWI inverts for the focal mechanism, depth and seismic moment, holding fixed the input epicentre. Centroid is then retrieved at the second step. Because event A is located close to stations, an incorrect epicentral input impacts the first step considerably, thus impacting the subsequent steps too. Care should be taken when studying earthquakes that simultaneously have large epicentral errors and are located close to stations. In case the earthquake is well recorded by several nearby stations, which is the case for onshore earthquakes in the present network geometry, no issue arises. The errors in epicentral locations that we tested are realistic for offshore events, but not for onshore events.

When the input starting depth is incorrect (Figs 3f–h), we observe a poor convergence toward true depth, especially when the 30-km starting depth is far from the true depth. This problem can be easily solved by iterating over different depths, as the misfit shows a clear minimum for the true depth. In applications with real data, we will evaluate a range of possible depths.

5 RESULTS AND DISCUSSION

The results obtained in this study are summarized in Table 4. From the total of 29 events studied, 12 had reliable solutions with quality factors A and B. Figs 4 and 5 display the results and data fits for an inversion of quality A (event 080111). The misfit for each source parameter is displayed using the relative misfit RM :

$$RM = \frac{(M - BM)}{BM}. \quad (3)$$

In eq. (3), M is the misfit for a given source parameter, and BM is the misfit obtained with the best-fitting parameter. Note that RM is always greater or equal to zero ($RM \geq 0$), with $RM = 0$ for the best-fitting source parameter ($M = BM$). Figs 4 and 5 show the

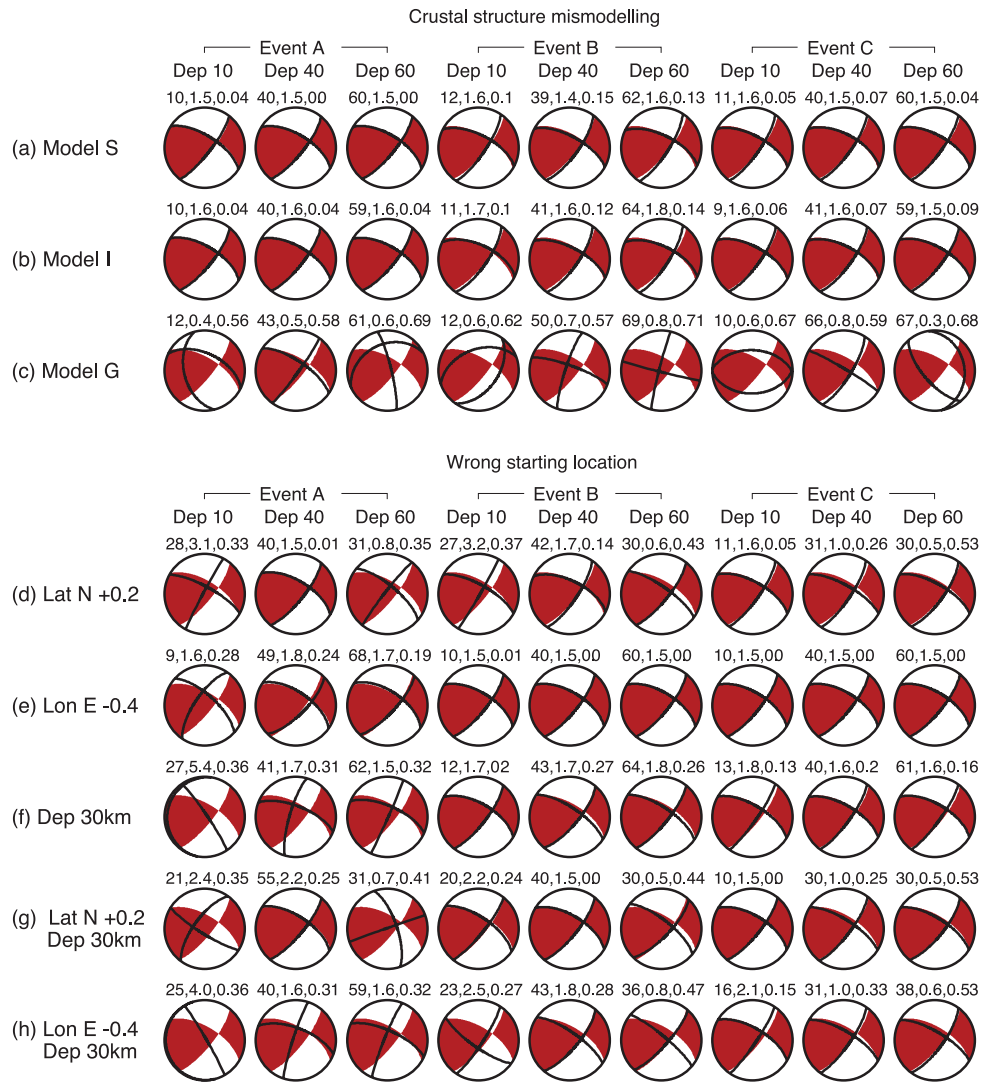


Figure 3. Summary of synthetic tests. The input focal mechanism is shown in red; the black lines show the retrieved focal mechanisms. The numbers above each focal mechanism indicate output depth (km), seismic moment ($\times 10^{15}$ N m) and misfit. We consider three earthquake epicentres (A, B and C) and three earthquake depths (10, 40 and 60 km). Rows (a)–(c): Effect of crustal mismodelling. ‘Perfect data’ are generated using crustal model S, and inverted using crustal models S, I and G (Fig. 2). Earthquake epicentre and depth are held fixed at their true values. Rows (d)–(h): Effect of incorrect starting location. (d) The starting epicentre is deviated with respect to the true epicentre by 0.2° N (approximately 20 km). (e) The starting epicentre is deviated by 0.4° W (approximately 35 km). In (d) and (e) the starting depth is held fixed at its true value. (f) The starting depth has an incorrect value of 30 km and the epicentre is held fixed at its true location; (g) and (h) represent the same situation as (d) and (e), that is, incorrect starting epicentres, now using also an incorrect starting depth of 30 km.

outputs and data fits from the first and second step of the inversion, respectively. At each step the inversion searches for all source parameters simultaneously. However, Figs 4 and 5 show only the variation of each individual parameter, while keeping all others fixed at their preferred value. Thus, these plots give only a limited image of the uncertainty of each parameter. To assess the robustness of each source parameter, we perform a bootstrap analysis with 100 different station configurations. The bootstrap analysis is simplified to keep the algorithm fast for real-time implementation. At the first step, bootstrap is performed by perturbing the source parameters around the best solution. The perturbation is not performed simultaneously for all source parameters, but rather for (1) scalar moment only; (2) depth only; and (3) strike, dip and rake simultaneously. At the second step, a true grid search on all parameters is performed simultaneously, while testing different station configurations. This bootstrap can be performed quickly because all misfits for individual traces were stored during the inversion. Thus, we simply recombine

the stored misfits. The probabilities of each source parameter, or combination thereof, based on bootstrap analysis, are shown in Table 4. These values correspond to lower bounds on true uncertainty, because: (1) they do not consider model error, solely data error, and (2) at step 1 a true bootstrap analysis is not performed, only a simplified bootstrap.

Fig. 6 compares the epicentres and depths reported in this study with those reported by IM, EMSC and Geissler *et al.* (2010, to which from now on we will refer simply as OBS). The epicentres given by IM, EMSC and OBS are all based on traveltimes. IM solutions are based on data collected by the Portuguese land network, EMSC on phases reported by different European networks, and OBS on data collected by a temporary deployment of 26 stations offshore (Geissler *et al.* 2010). The focal depths reported for a same event can differ significantly due to: (1) large azimuthal gap and distance to the nearest land stations, and/or (2) different crustal structures used for earthquake location. Fig. 6 shows that

Table 4. Epicentre, depth, magnitude, strike (Str), dip and rake (Rk) of the studied earthquakes. The probability of source parameters according to bootstrap analysis is shown between parenthesis (percentages indicate the probability for the bootstrap solutions to be within the intervals indicated in the table header). Also shown are the misfits obtained from step 1 (m_1) and step 2 (m_2), the number of waveforms and stations used in the inversion (Tr/St), and the quality of the solution (Q).

ID	M_w	M_0 (N m) ($\pm 0.1M_0$)	Latitude/longitude ($^{\circ}$ N/ $^{\circ}$ W) (± 2.5 km/ ± 2.5 km)	Depth (km) (± 10 km)	Str/Dip/Rk ($^{\circ}$ / $^{\circ}$ / $^{\circ}$) ($\pm 20^{\circ}$ / $\pm 20^{\circ}$ / $\pm 20^{\circ}$)	Str/Dip/Rk ($^{\circ}$ / $^{\circ}$ / $^{\circ}$) ($\pm 20^{\circ}$ / $\pm 20^{\circ}$ / $\pm 20^{\circ}$)	m_1	m_2	Tr/St	Q
070410	3.6	4.17e14 (97 per cent)	36.93 / 8.86 (70 per cent)	31.7 (100 per cent)	178 / 64 / -22 (83 per cent)	277 / 71 / -153	0.435	0.802	18/7	A
070701	4.5	1.09e16 (100 per cent)	36.55 / 12.06 (39 per cent)	33.9 (100 per cent)	98 / 65 / 148 (96 per cent)	202 / 61 / 28	0.34	0.876	18/8	A
080111 ^{OBS}	4.4	7.18e15 (93 per cent)	36.47 / 9.94 (68 per cent)	45.6 (100 per cent)	40 / 74 / 30 (99 per cent)	301 / 62 / 161	0.418	0.780	19/11	A
080414	3.6	3.56e14 (99 per cent)	37.3 / 9.31 (72 per cent)	29.7 (100 per cent)	201 / 77 / -19 (88 per cent)	295 / 71 / -166	0.405	0.850	26/11	B
081002	4.6	1.12e16 (93 per cent)	37.04 / 5.41 (70 per cent)	4.4 (100 per cent)	45 / 73 / 97 (97 per cent)	202 / 19 / 68	0.406	0.858	32/12	A
090217	3.4	2.33e14 (84 per cent)	38.07 / 8.57 (87 per cent)	13.2 (100 per cent)	28 / 74 / -5 (99 per cent)	120 / 85 / -164	0.437	0.799	26/10	A
090522	3.3	1.65e14 (100 per cent)	36.86 / 9.67 (63 per cent)	25 (100 per cent)	45 / 73 / 56 (88 per cent)	291 / 38 / 151	0.427	1.008	21/9	B
090705	4.1	2.62e15 (98 per cent)	36.04 / 10.44 (56 per cent)	40 (100 per cent)	225 / 54 / 0 (99 per cent)	315 / 90 / -144	0.378	0.568	14/8	A
091217	5.7	5.16e17 (100 per cent)	36.51 / 9.9 (34 per cent)	44.5 (100 per cent)	43 / 89 / 71 (100 per cent)	312 / 19 / 178	0.397	0.803	24/11	A
100331	3.7	6.12e14 (98 per cent)	36.76 / 9.76 (37 per cent)	24.9 (100 per cent)	62 / 74 / 64 (85 per cent)	303 / 31 / 147	0.414	1.024	20/10	B
100723	3.9	1.11e15 (100 per cent)	35.93 / 10.34 (77 per cent)	45 (100 per cent)	209 / 35 / -1 (79 per cent)	300 / 89 / -125	0.421	0.842	18/6	B
100725	3.8	8.35e14 (100 per cent)	36.23 / 7.71 (32 per cent)	24.7 (100 per cent)	158 / 46 / -48 (60 per cent)	285 / 57 / -125	0.414	1.018	23/8	B

OBS: Events that were recorded by an OBS temporary network (Geissler *et al.* 2010).

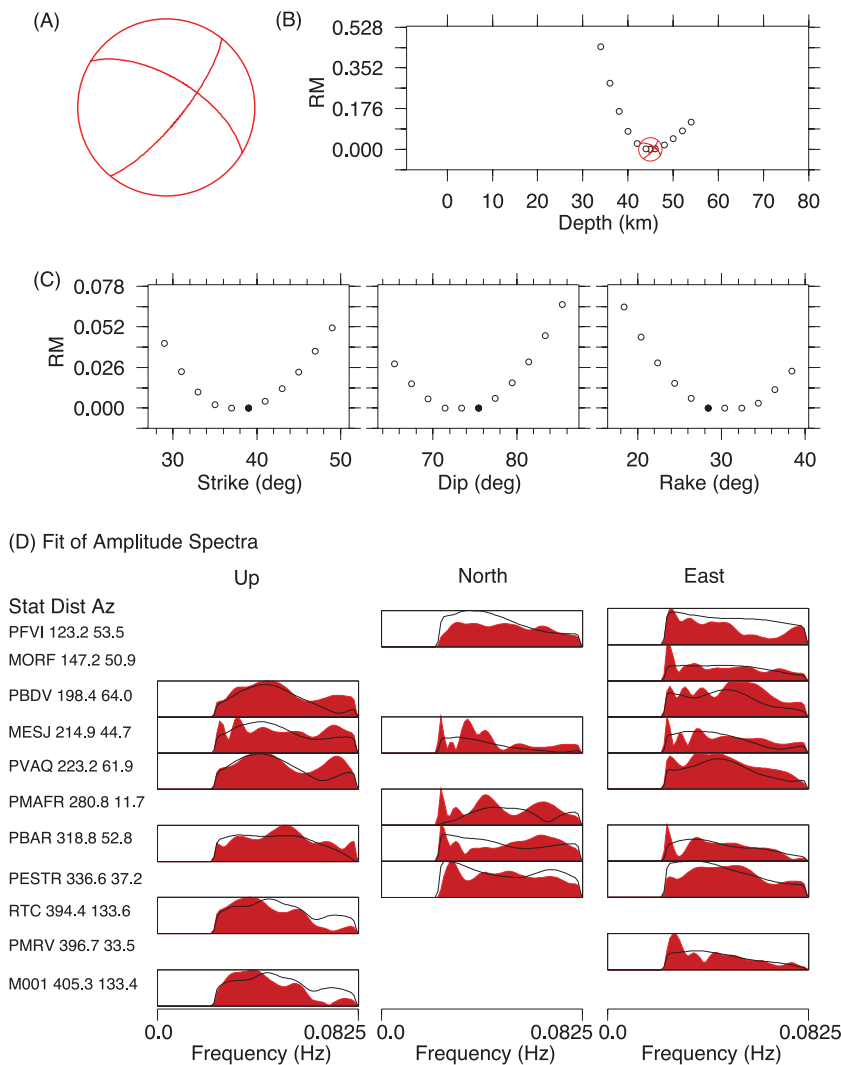


Figure 4. Output of KIWI step 1 for the 080111 event (quality A). (A) Preferred focal mechanism. Note that the compressive and dilatational quadrants are not determined. (B and C) Curves of relative misfit (RM) obtained by varying individual source parameters. Black dots mark the best point-source parameters. (D) Comparison between observed (red) and synthetic (black line) amplitude spectra. Labels on the left column indicate station names, distance to epicentre (km) and azimuth to epicentre ($^{\circ}$). All spectra are normalized. The amplitudes of the waveform are shown in Fig. 5.

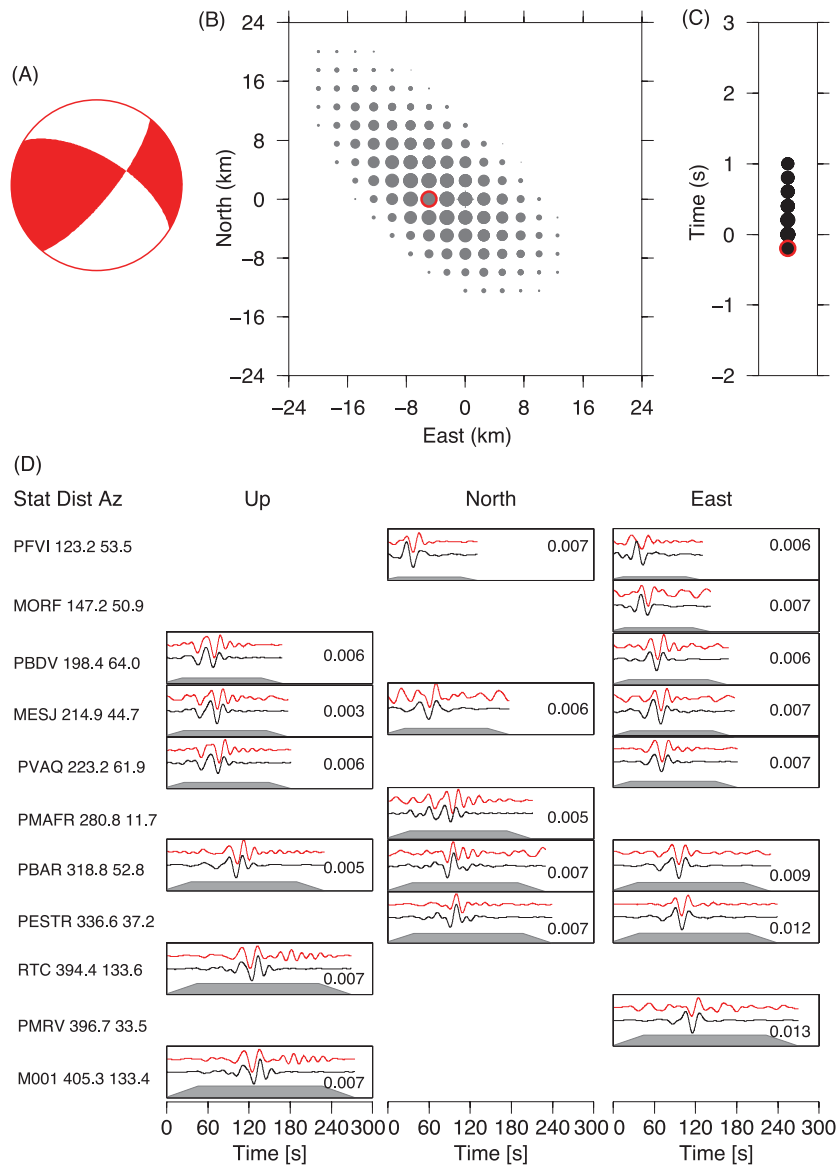


Figure 5. Output of KIWI step 2 for the 080111 event (quality A). (A) Preferred focal mechanism. The compressive/dilatational quadrants are now retrieved. (B) Centroid location and (C) origin time with respect to initial assumptions (crosses). The size of the grey circles scales with misfits for the tested locations and origin times. Red circles mark the best solutions. (D) Comparison between observed (red) and synthetic (black) waveforms. Labels on the left column indicate station names, distance to epicentre (km) and azimuth to epicentre ($^{\circ}$). The numbers next to the waveforms are the maximum amplitude in millimetres.

earthquake depths inferred with the KIWI tools are normally larger than those provided by IM (Preliminary Seismic Information 2010). This trend is consistent with that reported by Geissler *et al.* (2010), who locate most earthquakes at depths of 40–60 km. In general, our results indicate shallow earthquakes onshore (down to 13 km) and deeper earthquakes offshore (25–46 km). Our earthquake centroids are in general good agreement with IM epicentres, which is likely due to (1) the similarity of crustal models used on this study and by IM in traveltime analysis, and (2) the assumption on our first step that IM's epicentres are correct. When the initial epicentre assumed in the first step is grossly incorrect, KIWI is not able to converge towards the true centroid in the second step. In this case, the bootstrap analysis yields very low probabilities for the centroid (<30 per cent) and the solutions are considered unreliable.

Fig. 7 shows the moment magnitudes (M_w) inferred in this study versus the M_L magnitudes reported by IM, EMSC and OBS. The M_w obtained with KIWI are systematically lower than those reported by other institutions. In this study we estimate the seismic moment, hence the moment magnitude, from amplitude spectra of BB waveforms. The M_L scale used by IM was calibrated following Hutton & Boore (1987), using data recorded between 1996 and 2009 at the Portuguese network (Carrilho & Vales 2009). According to this calibration, an earthquake with $M_L = 2$ is defined as an earthquake that produces a maximum amplitude of 1 mm on a Wood-Anderson seismometer located 17 km away from the epicentre. Both the geometrical spreading and inelastic attenuation coefficients employed by IM for the Portuguese region are lower than those inferred by Hutton & Boore (1987) for California. Many studies have focused on the relation between M_w and M_L (e.g. Hanks & Boore 1984; Deichmann

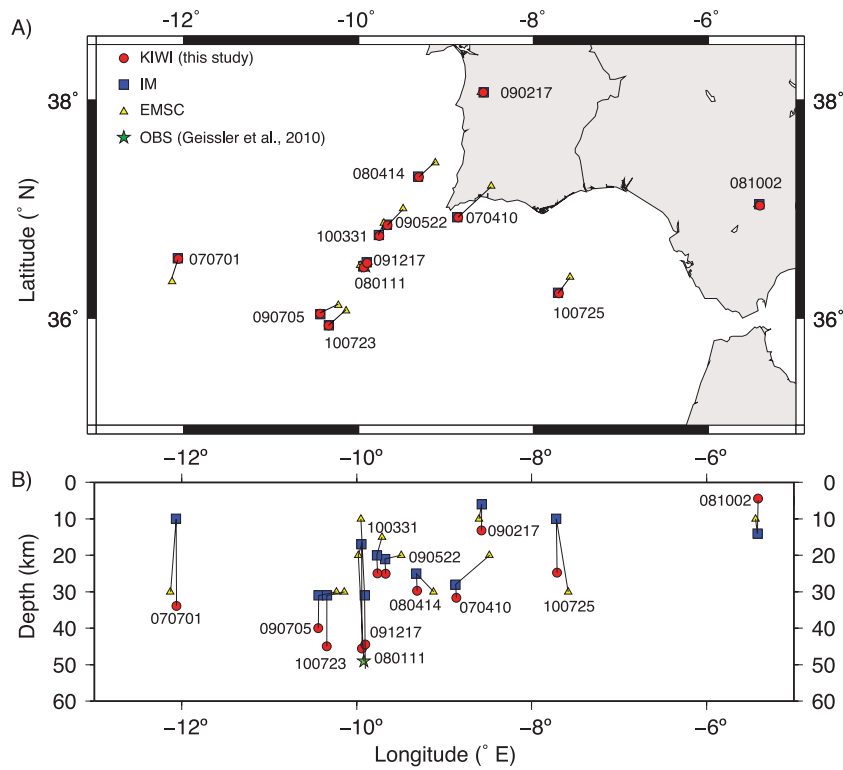


Figure 6. Comparison of epicentre and depths reported by this study (red circles), IM (blue squares), EMSC (yellow triangles) and OBS study of Geissler *et al.* (2010) (green stars). Only events of reliable qualities A and B are displayed.

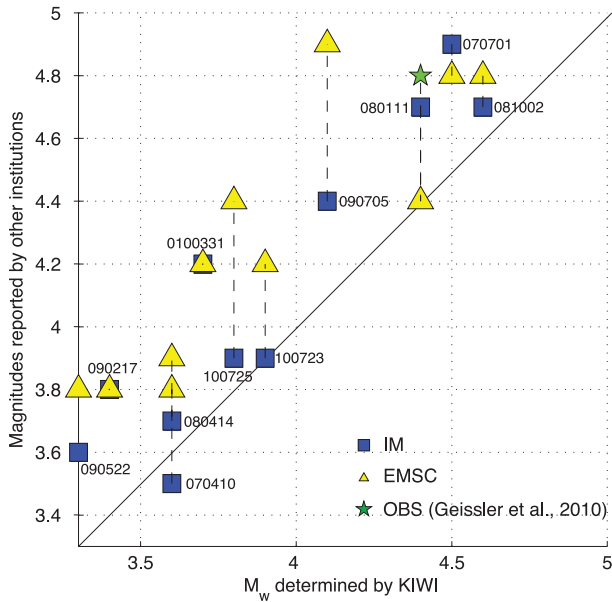


Figure 7. Local magnitudes (M_L) reported by different institutions versus magnitudes obtained in this study for earthquakes with $3.3 < M_w < 4.6$. The M_L values reported by IM (blue squares), EMSC (yellow triangles) and OBS study of Geissler *et al.* (2010) (green stars) are generally larger than the M_w we obtain, with EMSC reporting the highest magnitudes.

2006; Grünthal *et al.* 2009; Bethmann *et al.* 2011, and references therein). In general, $M_L \sim m M_w$, and m varies between 1 and 1.9, with higher m values for weaker events. For earthquakes in the magnitude range studied in this paper ($M_L > 3.5$), m is typically close to one. The systematic deviation between M_w and M_L in the Portuguese re-

gion deserves attention and should be further investigated in future studies.

Fig. 8 shows the focal mechanisms obtained in this study along with previously published focal mechanisms. Our solutions compare well with previous studies with the exception of event 100331. Event 100331, located offshore SW Portugal, is well constrained by the data and the focal mechanism compares well with neighbour events. However, it is an M_w 3.7 event located offshore, with limitations on the signal-to-noise ratio (hence its quality B). Also, the bootstrap probability for its centroid is low (37 per cent), indicating uncertainty in the solution. Event 091217, the largest event on the data set, was attributed M_L 6.0 by IM and was recorded with an excellent coverage, generating a quality A solution that compares well with those reported by the Global Centroid Moment Tensor (GCMT) project and INGV, while IGN reports a disparate solution for this event. In general, we consider solutions with quality A very reliable and quality B solutions acceptable. The focal mechanisms that we obtain indicate faulting styles which are dominantly thrust, strike-slip, and a mix of both. The two conjugate faulting planes are normally oriented NW–SE and NE–SW. These results are in good agreement with previous studies (e.g. Buforn *et al.* 1988, 1995, 2004; Borges *et al.* 2001; Stich *et al.* 2003, 2010).

Fig. 8 also displays the epicentres of earthquakes that we tried to model but with no success (qualities C and D). It is interesting to note that all earthquakes located south of station PBDV, within the the Cadiz sedimentary basin, cannot be successfully modelled. In fact, the data generated by these earthquakes are strongly affected by reverberation, which we cannot properly model with a 1-D crustal model. Most other unsuccessful inversions concern earthquakes located far from the network and/or earthquakes of low magnitude. Some of these earthquakes are not suitable for automated inversion

Data for this study were generously provided by Instituto de Meteorologia (PM); Instituto Dom Luiz (LX); Western Mediterranean Network (WM); Centro de Geofísica de Évora, Real Instituto y Observatorio de la Armada, Universidad Complutense de Madrid; Instituto Andaluz de Geofísica (IG); IberArray, project TopoIberia (IB); GEOFON, GEOForschungsNetz (GE); IRIS/USGS Network (IU); and MEDNET, Istituto Nazionale di Geofísica e Vulcanologia (MN).

The KIWI tools are available at <http://kinherd.org/>. We used the software SAC (Goldstein *et al.* 2003) for data pre-processing and GMT (Wessel & Smith 1998) for figure plotting. S. Custódio is supported by a Marie Curie International Reintegration Grant within the 7th European Community Framework Programme (PIRG03-GA-2008-230922). S. Cesca received funding from the BMBF project MINE (Programme GEOTECHNOLOGIEN, Grant of project BMBF03G0737).

REFERENCES

- Aki, K. & Richards, P. G., 1980. *Quantitative Seismology*, W. H. Freeman, San Francisco, ISBN 0716710587.
- Argus, D.F., Gordon, R.G., Demets, C. & Stein, S., 1989. Closure of the Africa-Eurasia-North America plate motion circuit and tectonics of the Gloria fault, *J. geophys. Res.*, **94**, 5585–5602.
- Bethmann, F., Deichmann, N. & Mai, P.M., 2011. Scaling relations of local magnitude versus moment magnitude for sequences of similar earthquakes in Switzerland, *Bull. seism. Soc. Am.*, **101**(2), 515–534.
- Borges, J.F., Fitas, A.J.S., Bezzeghoud, M. & Teves-Costa, P., 2001. Seismotectonics of Portugal and its adjacent Atlantic area, *Tectonophysics*, **331**, 373–387.
- Buforn, E., Udías, A. & Colombas, M.A., 1988. Seismicity, source mechanisms and tectonics of the Azores-Gibraltar plate boundary, *Tectonophysics*, **152**, 89–118.
- Buforn, E., Sanz de Galdeano, C. & Udías, A., 1995. Seismotectonics of the Ibero-Maghrebian region, *Tectonophysics*, **248**(3–4), 247–261.
- Buforn, E., Bezzeghoud, M., Udías, A. & Pro, C., 2004. Seismic sources on the Iberia-African plate boundary and their tectonic implications, *Pure appl. Geophys.*, **161**, 623–646.
- Calais, E., Demets, C. & Nocquet, J.-M., 2003. Evidence for a post-3.16-Ma change in Nubia-Eurasia-North America plate motions? *Earth planet. Sci. Lett.*, **216**, 81–92.
- Carrilho, F. & Vales, D., 2009. Modernization of the National Seismic Network, *6th Symposium of the Portuguese Association of Meteorology and Geophysics*, Vol. 77, Caparica, Portugal.
- Carrilho, F., Pena, A., Nunes, J. & Senos, M.L., 2004. Instrumental Earthquake Catalogue 1970–2000, Tech. Rep., Instituto de Meteorology, ISBN: 972-9083-12-6, Depsito Legal No: 221 955/05.
- Cesca, S., Buforn, E. & Dahm, T., 2006. Amplitude spectra moment tensor inversion of shallow earthquakes in Spain, *Geophys. J. Int.*, **166**, 839–854.
- Cesca, S., Heimann, S., Stammler, K. & Dahm, T., 2010. Automated procedure for point and kinematic source inversion at regional distances, *J. geophys. Res.*, **115**(B14), B06304, doi:10.1029/2009JB006450.
- Custódio, S., Cesca, S. & S., H., 2012. Fast kinematic waveform inversion and robustness analysis: application to the 2007 Mw 5.9 Horseshoe Abyssal Plain earthquake offshore southwest Iberia, *Bull. seism. Soc. Am.*, **102**(1), 361–376.
- Deichmann, N., 2006. Local magnitude, a moment revisited, *Bull. seism. Soc. Am.*, **96**(4A), 1267–1277.
- DeMets, C., Gordon, R.G., Argus, D.F. & Stein, S., 1994. Effect of recent revisions to the geomagnetic reversal time scale on estimates of current plate motions, *Geophys. Res. Lett.*, **21**, 2191–2194.
- Díaz, J. *et al.*, 2010. Background noise characteristics at the Iber array broadband seismic network, *Bull. seism. Soc. Am.*, **100**(2), 618–628.
- Fernandes, R.M.S., Ambrosius, B.A.C., Noomen, R., Bastos, L., Wortel, M.J.R., Spakman, W. & Govers, R., 2003. The relative motion between Africa and Eurasia as derived from ITRF2000 and GPS data, *Geophys. Res. Lett.*, **30**(16), 160000–160001.
- Fernandes, R.M.S., Miranda, J.M., Meijninger, B.M.L., Bos, M.S., Noomen, R., Bastos, L., Ambrosius, B.A.C. & Riva, R.E.M., 2007. Surface velocity field of the Ibero-Maghrebian segment of the Eurasia-Nubia plate boundary, *Geophys. J. Int.*, **169**, 315–324.
- Fukao, Y., 1973. Thrust faulting at a lithospheric plate boundary the Portugal earthquake of 1969, *Earth planet. Sci. Lett.*, **18**, 205–216.
- Geissler, W.H. *et al.*, 2010. Focal mechanisms for sub-crustal earthquakes in the Gulf of Cadiz from a dense OBS deployment, *Geophys. Res. Lett.*, **37**, L18309, doi:10.1029/2010GL044289.
- Giardini, D., Boschi, E. & Palombo, B., 1993. Moment tensor inversion from MEDNET data. II—regional earthquakes of the Mediterranean, *Geophys. Res. Lett.*, **20**, 273–276.
- Gilbert, F., 1971. Excitation of the normal modes of the Earth by earthquake sources, *Geophys. J. Int.*, **22**, 223–226.
- Goldstein, P., Dodge, D., Firpo, M. & Minner, L., 2003. Sac2000: signal processing and analysis tools for seismologists and engineers, in *Invited Contribution to The IASPEI International Handbook of Earthquake and Engineering Seismology*, eds Lee, W.H.K., Kanamori, H., Jennings, P.C. & Kisslinger, C., Academic Press, London.
- Grünthal, G., Wahlström, R. & Stromeyer, D., 2009. The unified catalogue of earthquakes in central, northern, and northwestern Europe (CENEC)—updated and expanded to the last millennium, *J. Seismol.*, **13**, 517–541.
- Hanks, T.C. & Boore, D.M., 1984. Moment-magnitude relations in theory and practice, *J. geophys. Res.*, **89**(B7), 6229–6235.
- Haskell, N.A., 1953. The dispersion of surface waves on multilayered media, *Bull. seism. Soc. Am.*, **43**, 17–34.
- Heimann, S., 2011. A robust method to estimate kinematic earthquake source parameters, *PhD thesis*, University of Hamburg, Hamburg, Germany, 161 p.
- Hutton, L.K. & Boore, D.M., 1987. The ML scale in southern California, *Bull. seism. Soc. Am.*, **77**(6), 2074–2094.
- Johnston, A.C., 1996. Seismic moment assessment of earthquakes in stable continental regions? III. New Madrid 1811–1812, Charleston 1886 and Lisbon 1755, *Geophys. J. Int.*, **126**, 314–344.
- Martinez Solares, J.M. & Lopez Arroyo, A., 2004. The great historical 1755 earthquake. Effects and damage in Spain, *J. Seismol.*, **8**, 275–294.
- McClusky, S., Reilinger, R., Mahmoud, S., Ben Sari, D. & Tealeb, A., 2003. GPS constraints on Africa (Nubia) and Arabia plate motions, *Geophys. J. Int.*, **155**, 126–138.
- McKenzie, D., Jackson, J. & Priestley, K., 2005. Thermal structure of oceanic and continental lithosphere, *Earth planet. Sci. Lett.*, **233**(3–4), 337–349.
- Nakanishi, I., Moriya, T., Endo, M. & Motoya, Y., 1992. The November 13, 1990 earthquake off the coast of the Primorskij region, the eastern Russia, *Geophys. Res. Lett.*, **19**, 549–552.
- Nocquet, J. & Calais, E., 2004. Geodetic measurements of crustal deformation in the western Mediterranean and Europe, *Pure appl. Geophys.*, **161**, 661–681.
- Pena, A., Nunes, C. & Carrilho, F., 2012. Catálogo Sísmico Instrumental 1961–1969, Tech. Rep., Instituto de Meteorologia.
- Preliminary Seismic Information, 2010. Boletins Sis-mológicos Mensais, Tech. Rep., Instituto de Meteorologia. [<http://www.meteo.pt/en/publicacoes/tecnico-cientif/noIM/boletins/>]
- Ritsema, J. & Lay, T., 1993. Rapid source mechanism determination of large ($M_w \geq 5$) earthquakes in the western United States, *Geophys. Res. Lett.*, **20**, 1611–1614.
- Serpelloni, E., Vannucci, G., Pondrelli, S., Argnani, A., Casula, G., Anzidei, M., Baldi, P. & Gasperini, P., 2007. Kinematics of the Western Africa-Eurasia Plate boundary from focal mechanisms and GPS data, *Geophys. J. Int.*, **169**(3), 1180–1200.

- Stich, D., Ammon, C.J. & Morales, J., 2003. Moment tensor solutions for small and moderate earthquakes in the Ibero-Maghreb region, *J. geophys. Res. (Solid Earth)*, **108**, 2148, doi:10.1029/2002JB002057.
- Stich, D., Mancilla, F.d.L., Pondrelli, S. & Morales, J., 2007. Source analysis of the February 12th 2007, M_w 6.0 Horseshoe earthquake: implications for the 1755 Lisbon earthquake, *Geophys. Res. Lett.*, **34**, L12308, doi:10.1029/2007GL030012.
- Stich, D., Martn, R. & Morales, J., 2010. Moment tensor inversion for Iberia-Maghreb earthquakes 2005-2008, *Tectonophysics*, **483**(3-4), 390-398.
- Thiebot, E. & Gutscher, M.-A., 2006. The gibraltar arc seismogenic zone (part 1): constraints on a shallow east dipping fault plane source for the 1755 Lisbon earthquake provided by seismic data, gravity and thermal modeling, *Tectonophysics*, **426**(1-2), 135-152.
- Thomson, W.T., 1950. Transmission of elastic waves through a stratified solid medium, *J. appl. Phys.*, **21**, 89-93.
- Vilanova, S.P. & Fonseca, J.F.B.D., 2007. Probabilistic seismic-hazard assessment for Portugal, *Bull. seism. Soc. Am.*, **97**(5), 1702-1717.
- Wang, R., 1999. A simple orthonormalization method for stable and efficient computation of Green's functions, *Bull. seism. Soc. Am.*, **89**, 733-741.
- Wessel, P. & Smith, W.H.F., 1998. New, improved version of Generic Mapping Tools released, *EOS, Trans. Am. geophys. Un.*, **79**(47), 579pp.
- Zitellini, N. *et al.*, 2009. The quest for the Africa-Eurasia plate boundary west of the Strait of Gibraltar, *Earth planet. Sci. Lett.*, **280**, 13-50.